Combining pressure and electrochemistry to synthesize superhydrides

Pin-Wen Guan[a], Russell J. Hemley[b,c,1], and Venkatasubramanian Viswanathan[a,d,1]

[a]Department of Mechanical Engineering, Carnegie Mellon University, Pittsburgh, PA 15213; [b]Department of Physics, University of Illinois Chicago, Chicago, IL 60607; [c]Department of Chemistry, University of Illinois Chicago, Chicago, IL 60607; and [d]Department of Physics, Carnegie Mellon University, Pittsburgh, PA 15213

Edited by Alexis T. Bell, University of California, Berkeley, CA, and approved October 5, 2021 (received for review June 7, 2021)

Recently, superhydrides have been computationally identified and subsequently synthesized with a variety of metals at very high pressures. In this work, we evaluate the possibility of synthesizing superhydrides by uniquely combining electrochemistry and applied pressure. We perform computational searches using density functional theory and particle swarm optimization calculations over a broad range of pressures and electrode potentials. Using a thermodynamic analysis, we construct pressure–potential phase diagrams and provide an alternate synthesis concept, pressure–potential ($\mathscr{P}^2$), to access phases having high hydrogen content. Palladium–hydrogen is a widely studied material system with the highest hydride phase being Pd_3H_4. Most strikingly for this system, at potentials above hydrogen evolution and $\sim$ 300 MPa pressure, we find the possibility to make palladium superhydrides (e.g., PdH_{10}). We predict the generalizability of this approach for La-H, Y-H, and Mg-H with 10- to 100-fold reduction in required pressure for stabilizing phases. In addition, the $\mathscr{P}^2$ strategy allows stabilizing additional phases that cannot be done purely by either pressure or potential and is a general approach that is likely to work for synthesizing other hydrides at modest pressures.

metal superhydrides | structure search | Pourbaix diagram | hydrogen loading

Hydrides are a large class of materials containing hydrogen, the lightest and most abundant element in the universe. They have attracted much research interest due to their scientific significance and numerous applications. As important hydrogen storage media (1), they are able to store hydrogen at densities higher than that of liquid hydrogen (2). They also find applications in hydrogen compressors (3), refrigeration (4), heat storage (5), thermal engines (6), batteries (7), fuel cells (8), actuators (9), gas sensors (10), smart windows (11), H_2 purification (12), isotope separation (13), alloy processing (14), catalysis (15), semiconductors (16), neutron moderators (17), low-energy nuclear reactions (18), and recently possible high-temperature superconductors with a critical superconducting temperature T_c in the vicinity of room temperature in hydrogen-rich materials under pressure (19–38).

In the late 1960s, Neil Ashcroft (19) and Vitaly Ginzburg (20) independently considered the possibility of high-temperature superconductivity in metallic solid hydrogen at high pressure. Later, the idea of chemical precompression was proposed in which chemical "pressure" is exerted to form hydrogen dominant metal hydrides stable at lower pressures (21). Following the successful prediction (22, 23) and confirmation (24) of very high T_c superconductivity in H_3S, near–room-temperature superconductivity was predicted (25, 26), synthesized (27), and discovered (28) in the superhydrides (defined as MH_n, for $n > 6$) in the La-H system. Later, comparable T_c values were observed experimentally for other La-H (29), Y-H (30–32), and La-Y-H (33) superhydrides, and room-temperature superconductivity was also reported in the C-S-H system (34). In addition, even higher T_c s have been theoretically predicted, such as Li_2MgH_{16} with T_c as high as $\sim$ 470 K at 250 GPa (35).

High pressures are needed to synthesize superhydrides (38). One major reason is that at lower pressures, the thermodynamic stability of superhydrides is weakened or no longer exists. To overcome such a challenge, it is obvious that more processing variables need to be introduced in addition to chemical composition and pressure. A processing variable that has been largely hidden is the electrical potential when utilizing electrochemistry for synthesis, which has been used in synthesizing palladium hydride at ambient pressure (39). In the present work we show that the synergetic use of pressure and electrical potential can dramatically extend the thermodynamic stability regime of superhydrides to modest pressures, an approach we term $\mathscr{P}^2$. This approach opens more opportunities for the creation of superhydrides and other materials by combining pressure and electrochemical loading techniques. We begin by outlining the general thermodynamic framework. We then apply the approach to the Pd-H system, where we also present density functional theory (DFT) predictions of palladium hydrides under pressure. This is followed by predictions for other metal hydride systems and then a discussion of the broad implications.

Pressure–Potential Hydride Synthesis

Superhydrides were first documented experimentally using megabar high-pressure diamond-anvil cell laser-heating techniques, leading to the discovery of near–room-temperature superconductivity in LaH_{10} (27, 28, 36). This result was subsequently confirmed (29), and other metal superhydrides

Significance

Superhydrides are a materials system where near–room-temperature superconductivity has been achieved but only at very high (megabar) pressures. This work proposes an approach that combines pressure and electrochemistry to stabilize superhydrides at moderate pressures. Through a computational study of the palladium–hydrogen system, we construct electrochemical phase diagrams and show that electrochemically synthesizing superhydrides may be possible when combined with moderate pressures. We generalize this to other binary metal superhydrides of interest for superconductivity, including La, Y, and Mg hydrides.

Author contributions: P.-W.G., R.J.H., and V.V. designed research; P.-W.G. performed research; P.-W.G., R.J.H., and V.V. analyzed data; and P.-W.G., R.J.H., and V.V. wrote the paper.

Competing interest statement: P.-W.G. and V.V. are inventors on a patent application related to electrochemical synthesis of metal superhydrides.

This article is a PNAS Direct Submission.

[1]To whom correspondence may be addressed. Email: venkvis@cmu.edu or rhemley@uic.edu.

This article contains supporting information online at https://www.pnas.org/lookup/suppl/doi:10.1073/pnas.2110470118/-/DCSupplemental.

Published November 9, 2021.

have subsequently been observed (30–33, 37). We now discuss an alternate pressure–potential approach, $\mathscr{P}^2$, to synthesize dense metal hydrides, including superhydrides, by combining pressure and electrochemistry (i.e., electrode potential). In the $\mathscr{P}^2$ approach, an electrode consisting of a metal (or conducting metal hydride) is loaded with hydrogen by holding at an appropriate electrode potential using an electrolyte consisting of mobile protons. The proton-conducting membrane could be an aqueous electrolyte solution, a polymer electrolyte membrane (e.g., Nafion) (39), proton-conducting ceramic electrolytes (39), or solid acid proton conductors (40). The electrolytes provide a way to tune the activity of mobile protons and kinetics of reactions at electrode–electrolyte interfaces.

The hydrogen loading reaction for a metal electrode M (e.g., Pd) and an electrolyte containing mobile protons H^+ with electrons e^- involved and MH_n as the product is given by

$$M + n(H^+ + e^-) \Longleftrightarrow MH_n, \quad [1]$$

with the associated Gibbs energy change of the reaction:

$$\Delta G = G_{MH_n} - G_M - nG_{H^+} - nG_{e^-}. \quad [2]$$

The Gibbs energy of protons in the electrolyte is dependent on their activity a_{H^+}, which is a measure of their "effective concentration"

$$G_{H^+} = G_{H^+(a_{H^+}=1)} + k_B T \ln(a_{H^+}), \quad [3]$$

where k_B and T are Boltzmann constant and temperature, respectively. The Gibbs energy of electrons is dependent on the electrode potential

$$G_{e^-} = G_{e^-(U=0)} - eU_{SHE}, \quad [4]$$

where e is the elementary charge, and U_{SHE} is the electrode potential referenced to the standard hydrogen electrode (SHE). The SHE reference is defined to satisfy the relation

$$G_{H^+(a_{H^+}=1)} + G_{e^-(U_{SHE}=0)} = G_{H(stable)}, \quad [5]$$

where $H(stable)$ denotes the stable phase of hydrogen that may be fluid or solid, depending on the pressure. Note that the conventional definition of SHE has no consideration for high pressure, and therefore it is modified here for convenience in high-pressure electrochemistry applicable to megabar regimes. It follows that

$$\Delta G = G_{MH_n} - G_M - nG_{H(stable)} + neU_{SHE} - nk_B T \ln(a_{H^+}). \quad [6]$$

This relation allows us to construct an electrochemical phase diagram for loading hydrogen into a material as a function of pH (i.e., $-\log_{10}(a_{H^+})$) and electrode potential. Lowering the electrode potential (making it more negative) or increasing the activity of protons (decreasing pH) enables loading higher amounts of hydrogen.

However, in a practical device, at negative potentials, metals tend to catalyze the hydrogen evolution reaction (HER) (41), given by

$$2H^+ + 2e^- \Longleftrightarrow H_2. \quad [7]$$

Hence, electrochemical loading needs to compete with the HER. Electrolyte formulations can suppress the HER kinetically through superconcentrated electrolytes (42) or other suppressing mechanisms. It is worth noting that in our analysis, we have to consider the generalized hydrogen evolution reaction, where at a given pressure the stable hydrogen phase needs to be considered, given by

$$H^+ + e^- \Longleftrightarrow H_{stable}. \quad [8]$$

However, we set the limit for electrochemical synthesizability at the potential where reaction free energy for HER on the catalyst surface is thermodynamically downhill, which is determined by the free energy of adsorbed hydrogen on the metal surface (41). While the $\mathscr{P}^2$ approach is demonstrated with a proton conductor, a similar scheme can be constructed with hydride ion conductors (43) (for, e.g., $M + nH^- \Longleftrightarrow MH_n + ne^-$.

In addition to suppressing hydrogen evolution, pressure also modifies the proton transport by suppressing thermal motion of protons in the hydrides (44, 45). Pressure can modulate the local strain field in the solids, which is another important factor affecting the transport of atoms in both the electrode (46) and the electrolyte (47, 48). Strong local distortion promotes formation of proton polarons and increases the proton activation energy and, thereby, decreases the proton mobility (47, 48).

Application to the Pd-H System

We first study the example of the Pd-H system. As Pd catalyzes the competing HER at very low overpotential (41), this system can serve as a limiting case for the approach. The calculations of Gibbs energies of relevant phases necessitate information about their crystal structures. Experimentally, the highest hydride phase found so far is Pd_3H_4 (49), which was synthesized at around 5 GPa and crystallized in the structure with a face-centered cubic (fcc) H lattice intercalated with a Pd/vacancy fcc lattice in the Cu_3Au-type ordering. Possible Pd hydrides with even higher hydrogen content have apparently not yet been reported. Therefore, a DFT structure search using particle swarm optimization (PSO) is used to explore possible crystal structures of Pd hydrides with different compositions (*SI Appendix*).

Ground-state structures are shown in Fig. 1 for selected compositions and pressures; additional structures can be found in *SI Appendix* and the Github repository. In PdH and Pd_3H_4 structures, all the H atoms are bonded to the Pd atoms. We predict the rocksalt structure with the $Fm\bar{3}m$ space group as the ground state of PdH at high pressure, consistent with experiments (50, 51). However, the predicted ground state at low pressure is calculated to have an $R3m$ structure, not the experimentally found rocksalt structure. This may be attributed to lack of consideration for higher-level effects such as the quantum or anharmonic effects. For the Pd superhydrides, the structures consist of Pd-H layers or clusters between which H_2 molecules are located.

To more quantitatively characterize the structural features of these Pd hydrides, a bond topology analysis of the low-enthalpy structures was performed (Fig. 2). Both pressure and composition have significant influence on the coordination number (CN) of Pd and the dimensionality of the Pd-H framework. At zero pressure, the CN is between 3 and 7 and has moderate variation with composition. The dimensionality changes around PdH_2 sharply. From PdH to PdH_2, the frameworks are exclusively three-dimensional (3D). From PdH_3 to PdH_6, the frameworks are exclusively two-dimensional (2D), while starting from PdH_7, both one-dimensional (1D) and 2D frameworks exist. At 150 GPa, the frameworks are invariably 3D regardless of the compositions, but CN spans between 5 and 18 and shows a dramatic change with composition. More analysis about the obtained structures of Pd hydrides can be found in *SI Appendix*.

The phase stability of the identified structures in the Pd-H system is assessed using the Bayesian error estimation functional with van der Waals correlation (BEEF-vdW) (52), which contains an ensemble of functionals distributed around the best-fit one to avoid bias from exchange-correlation errors (details in *Materials and Methods*). We find that the approach predicts no thermodynamically stable Pd superhydrides at both ambient and megabar conditions (*SI Appendix*, Figs. S11 and S12), although the stability of superhydrides is significantly increased at megabar

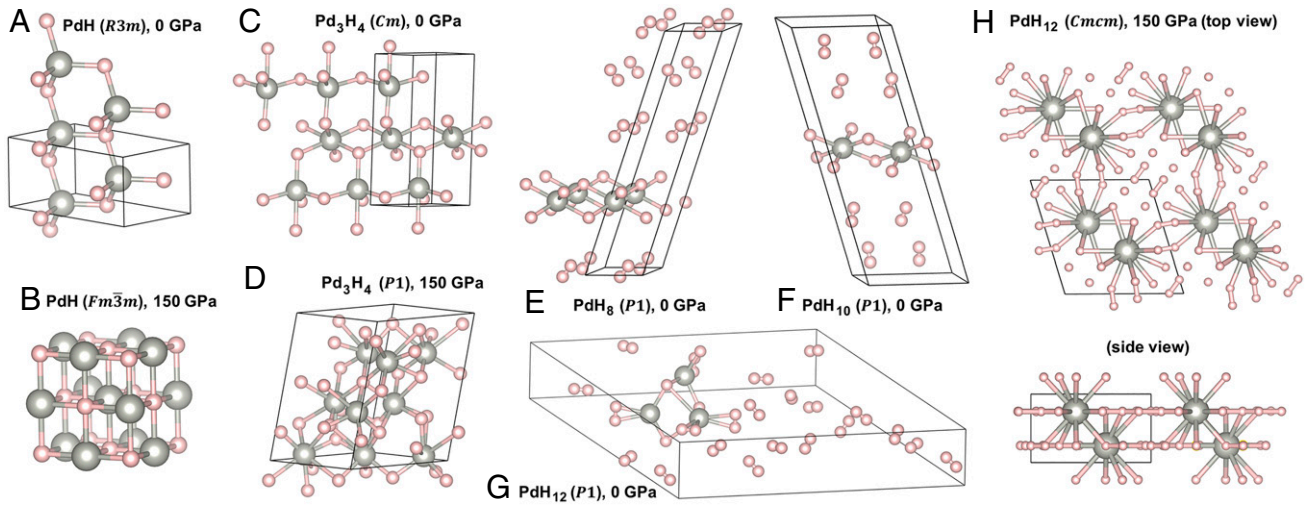

Fig. 1. Results of ground-state structure search for (*A*) PdH at 0 GPa, (*B*) PdH at 150 GPa, (*C*) Pd_3H_4 at 0 GPa, (*D*) Pd_3H_4 at 150 GPa, (*E*) PdH_8 at 0 GPa, (*F*) PdH_{10} at 0 GPa, (*G*) PdH_{12} at 0 GPa, and (*H*) PdH_{12} at 150 GPa. The gray balls represent Pd atoms, and the pink balls represent H atoms. The space groups of the corresponding structures are indicated in parentheses.

conditions. Therefore, synthesizing Pd superhydrides using only pressure is challenging, if not impossible. This raises the intriguing question of whether palladium superhydrides could be synthesized by introducing an electrochemical environment and whether it can be done at modest pressures, e.g., at 100-MPa (kilobar) versus 100-GPa (megabar) conditions. Although electrochemical studies have been performed over the years in the 100-MPa range (maximum of 1 GPa) (53, 54), the field remains largely unexplored.

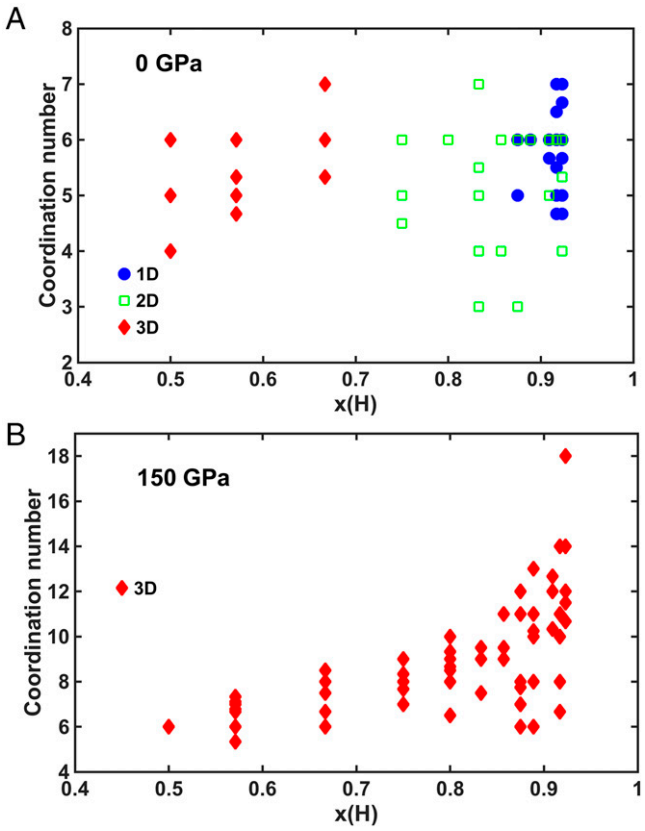

Fig. 2. Composition-dependent bond topological features of the low-enthalpy structures at (*A*) zero pressure and (*B*) 150 GPa. The coordination number corresponds to the number of nearest-neighbor H atoms surrounding a Pd atom, and the dimensionality is used to describe the framework formed by the Pd polyhedra.

To examine the possibility of stabilizing Pd superhydrides at modest pressures, we calculate a comprehensive pressure-dependent Pourbaix diagram at 300 K using the best-fit BEEF-vdW functional, with the reversible hydrogen electrode (RHE) as the reference (Fig. 3). Here the RHE reference is used instead of the SHE reference, since the former absorbs the potential change due to pH and makes the HER potential independent of pH, which is a more convenient choice for the present case. At decreasing potentials, the phase transition sequence is $\mathrm{Pd} \rightarrow \mathrm{PdH} \rightarrow \mathrm{PdH_{10}} \rightarrow \mathrm{PdH_{12}}$. At ambient pressure, we find that electrochemical loading of even the PdH phase is challenging and will compete with the HER, as observed experimentally (39). The most thermodynamically accessible Pd superhydride, PdH_{10} has a very narrow potential window near ambient pressure, which is gradually enlarged with increasing pressure. The phase boundary between PdH and PdH_{10}, can be fitted as the relation

$$\mathrm{U} = -0.168 + 0.0297 * \log_{10}(\mathrm{P}) + 8.83 * 10^{-5} \times \mathrm{P}^{2/3}, \quad [9]$$

where U is the electrode potential on the RHE scale (in volts) needed to transform PdH to PdH_{10} under a given pressure P (in megapascals). Near the ambient pressure, the above relation has good linearity between U and $\log_{10}$(P), and the power of the electrochemical driving force is illustrated by the fact that an order of magnitude reduction of the transition pressure can be achieved by only 0.03 V change in the electrode potential. When the pressure approaches 10^3 MPa (1 GPa), nonlinearity of the relation becomes significant. The region above the HER potential in Fig. 3 indicates the electrode potentials that are accessible without causing HER and therefore can be effectively utilized for hydride synthesis. The superhydride PdH_{10} is predicted to be stabilized at about 300 MPa (0.3 GPa) at the HER potential with the overpotential due to hydrogen adsorption taken into consideration. Using superconcentrated electrolytes that can suppress HER further, it is expected that PdH_{10} can be stabilized under even lower pressure operating at a more negative potential.

We provide a qualitative discussion of how a mere 0.03 V of potential change can reduce the transition pressure by an order of magnitude near the ambient pressure. In the low-pressure

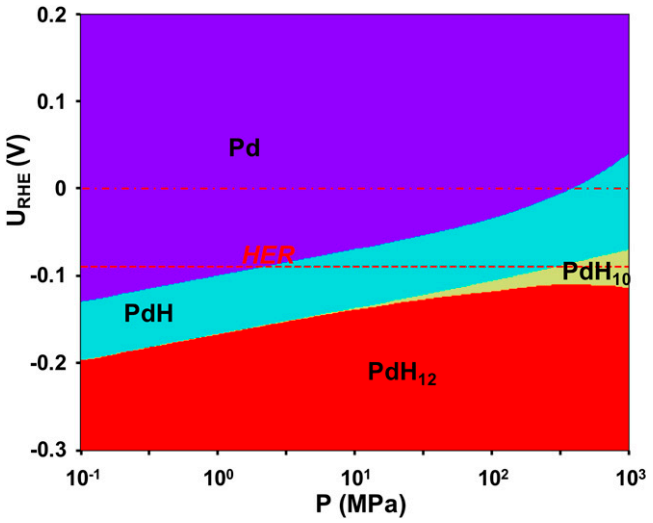

Fig. 3. Pressure-dependent Pourbaix diagram of Pd-H by the best-fit BEEF-vdW functional at 300 K. The dotted-dashed red line represents the equilibrium HER potential on Pd, while the dashed red line takes overpotential into consideration.

regime, the dominant effect of pressure is on the free energy of hydrogen gas, whose pressure-dependent part is $\frac{1}{2}k_B T \ln(P)$ (using the ideal gas approximation). This leads to a change of 0.0298 eV when changing the pressure by an order of magnitude at 300 K. This value well explains the coefficient of the $\log_{10}(P)$ term in the above-calculated phase boundary. The regimes beyond low pressure have more complicated pressure-dependent Gibbs energies for fluid and solid phases and require a more sophisticated treatment.

Application to Other Metal Hydride Systems

From an electrochemical synthesis standpoint, palladium is among the most difficult as it catalyzes HER with negligible overpotential (41). To demonstrate the generality of this strategy, the pressure-dependent Pourbaix diagrams were calculated for three other hydride systems, Y-H, Mg-H, and La-H (Fig. 4). In all these systems, high-temperature superconductors have been predicted or observed. Calculations similar to those above for Pd-H indicate that YH_9, MgH_{16}, and LaH_8 can be synthesized under ambient or modest pressure at potentials without HER. As for Pd-H, the critical potential becomes less negative with increasing pressure. The results for these different metal–hydrogen systems thus demonstrate that using electrochemistry to drastically lower the synthesis pressure of superhydrides is a general approach. It is also worth noting that, although superhydrides are emphasized in the present work, this approach can be applied to other hydrides as well, some of which also exhibit interesting properties such as room-temperature superconductivity in hole-doped H_3S (55).

Most notable are the results for La-H and the near–room-temperature superconducting phase LaH_{10} (28, 29, 36). The calculated stability up to 200 GPa for La-H shows a rich set of superhydrides, the stabilizing pressures of which are predicted to be significantly reduced (in tens of gigapascals) by the electrode potential above HER. For instance, LaH_{16} is predicted to be stabilized below 100 GPa at the HER potential while an extreme pressure above 200 GPa is needed without an electrochemical driving force. It is also noted that the experimentally verified LaH_{10} phase is stabilized only after removing LaH_{11} in the

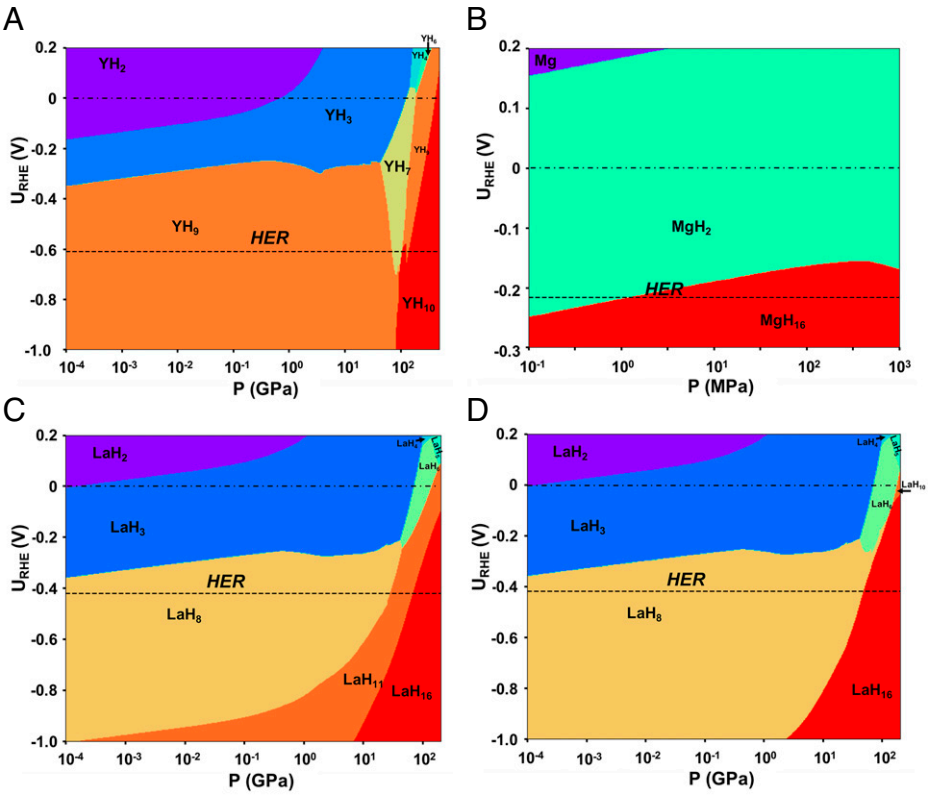

Fig. 4. Pressure-dependent Pourbaix diagram by the best-fit BEEF-vdW functional at 300 K: (*A*) Y-H, (*B*) Mg-H, and (*C* and *D*) La-H with LaH_{11} (*C*) and without LaH_{11} (*D*) considered. The dotted-dashed lines represent the equilibrium HER potential on the metal, while the dashed lines take overpotential into consideration.

underlying data, which may be due to the errors caused by neglecting higher-order corrections such as anharmonicity (44) and nuclear quantum effects (56) in the calculations. Such corrections usually enhance the stability of the high-density structures to lower pressures (44). More interestingly, the potential not only decreases the critical pressure, but also stabilizes some phases that cannot be stabilized regardless of pressure at zero potential, such as LaH_4, LaH_5, and LaH_8. Such an additional degree of freedom therefore opens up a broad materials space that has been largely unexplored.

Discussion

The above analysis based on pressure-dependent Pourbaix diagrams provides us with useful insights on how the interplay between electrochemistry and pressure can dramatically change stability of palladium hydrides. As in other structure search calculations (25, 26), crystal defects are not taken into consideration in the present calculations and therefore all the calculated phases are stoichiometric. On the other hand, a study of thermodynamic stability of PdHx under pressure in a nonelectrochemical environment shows that x increases to unity at about 2 GPa (57). Due to the approximations on stoichiometry, the calculated lower-bound pressure of the stability region of PdH at zero potential is several hundred megapascals, comparable to but lower than the experimental value. We also point out that the stability in this study is based on thermodynamics, while the dynamical stability may be quite different. For example, UH_7 is predicted to be thermodynamically unstable but dynamically stable at pressures below 22 GPa (58).

The observations of phase transitions are influenced by kinetics, and the thermodynamically stable phases may be difficult to access due to high kinetic barriers. Instead, metastable phases may form, depending on reaction pathways, as evident in electrochemical synthesis of intermetallics such as compounds found in the Na-Sn system (59). On the other hand, since the target phases stabilized by pressure and potential become unfavorable at normal conditions without compression and electrochemical environment, a sufficient energy barrier is needed to prevent the transition to the more stable phases when retrieving the target phases at normal conditions.

Due to these considerations, the phase diagrams presented here should be considered useful for understanding the large effect of electrochemical potential in stabilizing superhydrides at more modest pressures, instead of as precise predictions of synthesis conditions as a result of anharmonicity (44), quantum effects (56), or possible metastable behavior (59). It is hoped that the results stimulate additional calculations that take into account these effects as well as experimental verification of the predictions.

Conclusions

Using first-principles density functional theory and particle swarm structure search calculations, the phase stability of metal superhydrides has been studied. Focusing on the Pd-H system, we find from an analysis of the electrochemical loading of hydrogen in the metal under a broad range of pressures that it is possible to electrochemically synthesize PdH_{10} before the onset of hydrogen evolution. Remarkably this is predicted to occur at even modest pressures of about 300 MPa, which are readily accessible using existing high-pressure methods. Given that palladium is among the most active metals for hydrogen evolution, we suspected significant effects of electrochemical loading on the synthesis of other hydrides. Indeed, we demonstrate the generalizability of this pressure–potential ($\mathscr{P}^2$) approach for La-H, Y-H, and Mg-H, often yielding 10 to 100 times reduction in predicted pressure needed for stabilizing a particular phase, as well as stabilizing phases that cannot be done purely by either pressure or potential.

Combining pressure and electrochemistry thus offers a potential alternate route to synthesize metal superhydrides and other novel materials at currently accessible static pressure conditions, although further experimental and theoretical efforts are necessary to verify and refine the preliminary findings outlined here. Numerous extensions of existing electrochemical and high-pressure techniques could lead to altogether different materials created under an even broader range of pressures. This proof-of-concept work should serve to explore the frontier of high-pressure electrochemistry to produce novel materials with broad applications (18, 60).

Materials and Methods

Calculation Details. All DFT calculations involving the BEEF-vdW exchange correlation functional were run using GPAW software using the atomic simulation environment (ASE) (61–63). A real-space grid with spacing of 0.16 Å is used for the representation of electronic wavefunctions, and a k-point density of larger than 30 Å in reciprocal space was used in each dimension. For each material, the geometry is relaxed to a maximum force of less than 0.01 eV/Å. For the solid phases, the Gibbs energies include 0 K total energies and contributions from pressure, while the finite-temperature contributions are ignored. For each pressure, a Vinet equation of state (64) is fitted to find the equilibrium volume that should minimize the Gibbs energy, and the corresponding Gibbs energy is also determined at the same time. For the fluid hydrogen phases that have nonnegligible finite-temperature effects, the data from the National Institute of Standards and Technology database (65) are used. The HER overpotential is calculated based on the assumption that the HER kinetics are determined by the hydrogen adsorption on the electrode surface (41),

$$\Delta U^{HER} = |\Delta G_{H^*}| = |\Delta E_H + \Delta E_{ZPE} - T\Delta S_H| \approx |\Delta E_H + 0.24eV|, \quad [10]$$

where ΔG_{H^*} is the Gibbs energy change of hydrogen adsorption, ΔE_H is the hydrogen chemisorption energy, ΔE_{ZPE} is the difference in zero point energy between the adsorbed and the gas phase, and ΔS_H is the entropy change of hydrogen adsorption.

Structure Search. The particle swarm optimization is employed for structure search, using the CALYPSO (Crystal structure AnaLYsis by Particle Swarm Optimization) code (66, 67). Since only the superhydrides are of interest here, the searched compositions include PdH_n (n is an integer and $1 \leq n \leq 12$) and Pd_3H_4, which is the highest Pd hydride reported in experiments so far, totaling 13 compositions in all. For each composition, one unit cell is allowed to have one to four formulas. For a fixed number of formulas at a given composition, about 1,000 structures were searched during the structure evolution.

Bayesian Error Estimation Functional. For each material, a collection of functionals at the level of the generalized gradient approximation (GGA) were used as described below. Error estimation was carried out using the Bayesian error estimation functional with van der Waals correction (52). This empirically fitted functional generates an ensemble of functionals that are small perturbations away from the best-fit functional in exchange-correlation space.

The exchange-correlation energy for the BEEF-vdW is given in ref. 52 as

$$E_{xc} = \sum_m a_m \int \varepsilon_x^{UEG}(n) B_m[t(s)] d\mathbf{r} + \alpha_c E^{LDA-c} + (1-\alpha_c) E^{PBE-c} + E^{nl-c}. \quad [11]$$

Here B_m is the mth Legendre basis function, each of which has a corresponding expansion coefficient a_m. The expansion coefficients, as well as the α_c parameter that mixes the local density approximation (LDA) and Perdew–Burke–Ernzerhof (PBE) (68) exchange correlation functionals, have been prefitted with respect to a range of datasets as described in ref. 52. Additionally, within the functional is the E^{nl-c} nonlocal correlation term implemented via the vdW-DF2 (69) method. The method to generate the ensemble of functionals was tuned such that the spread of the predictions of the functionals matches the error of the main self-consistent functional with respect to the training and experimental data on which it was originally trained. Each of these functionals can then provide a non–self-consistent prediction of energy and therefore allows for a computationally efficient yet systematic way of understanding the sensitivity of the final prediction with respect to small changes in exchange-correlation functional.

Bond Topology Analysis. The coordination number is determined using the CrystalNN class based on a Voronoi algorithm in pymatgen (70). The framework of the crystal structure and its dimensionality are identified using the Zeo++ code based on the Voronoi decomposition (71), where radii of 0.5 and 1.6 Å are adopted for H and Pd, respectively.

Data Availability. The data that support the findings of this study and custom code for calculating and plotting the phase diagrams based on first-principles data presented in this paper are available on GitHub (https://github.com/BattModels/P2) (72).

ACKNOWLEDGMENTS. This work was partially supported by Google and by the Department of Energy-National Nuclear Security Administration (DOE/NNSA). R.J.H. acknowledges US NSF Grant DMR-1933622 and DOE/NNSA Grant DE-NA0003975. We thank Yet-Ming Chiang, Matt Trevithick, and Florian Metzler for helpful discussions.

1. B. Viswanathan, M. V. C. Sastry, S. S. Murthy, *Metal Hydrides: Fundamentals and Applications* (Springer, 1998).
2. L. Schlapbach, A. Züttel, Hydrogen-storage materials for mobile applications. *Nature* **414**, 353–358 (2001).
3. M. V. Lototskyy, V. A. Yartys, B. G. Pollet, R. C. Bowman Jr., Metal hydride hydrogen compressors: A review. *Int. J. Hydrogen Energy* **39**, 5818–5851 (2014).
4. P. Muthukumar, M. Groll, Metal hydride based heating and cooling systems: A review. *Int. J. Hydrogen Energy* **35**, 3817–3831 (2010).
5. A. Reiser, B. Bogdanović, K. Schlichte, The application of Mg-based metal-hydrides as heat energy storage systems. *Int. J. Hydrogen Energy* **25**, 425–430 (2000).
6. K. Nomura, Y. Ishido, S. Ono, A novel thermal engine using metal hydride. *Energy Convers.* **19**, 49–57 (1979).
7. R. Mohtadi, S.-i. Orimo, The renaissance of hydrides as energy materials. *Nat. Rev. Mater.* **2**, 1–15 (2016).
8. G. Sandrock, R. C. Bowman Jr., Gas-based hydride applications: Recent progress and future needs. *J. Alloys Compd.* **356**, 794–799 (2003).
9. K. Kurosaki *et al.*, Design and development of MH actuator system. *Sens. Actuators A Phys.* **113**, 118–123 (2004).
10. F. DiMeo Jr. *et al.*, MEMS-based hydrogen gas sensors. *Sens. Actuators B Chem.* **117**, 10–16 (2006).
11. S. Z. Karazhanov, A. Ulyashin, Similarity of optical properties of hydrides and semiconductors for antireflection coatings. *Philos. Mag.* **90**, 2925–2937 (2010).
12. F. Block, A. Dey, H. Kappes, K. Reith, Hydrogen purification with metal hydrides in a new kind of reactor. *J. Less Common Met.* **131**, 329–335 (1987).
13. A. S. Horen, M. W. Lee, Metal hydride based isotope separation–Large-scale operations. *Fusion Technol.* **21**, 282–286 (1992).
14. P. Sun *et al.*, An experimental study of the (Ti–6Al–4V)–xH phase diagram using in situ synchrotron XRD and TGA/DSC techniques. *Acta Mater.* **84**, 29–41 (2015).
15. H. Mimoun, Selective reduction of carbonyl compounds by polymethylhydrosiloxane in the presence of metal hydride catalysts. *J. Org. Chem.* **64**, 2582–2589 (1999).
16. S. Z. Karazhanov, A. Ulyashin, P. Vajeeston, P. Ravindran, Hydrides as materials for semiconductor electronics. *Philos. Mag.* **88**, 2461–2476 (2008).
17. J. Vetrano, Hydrides as neutron moderator and reflector materials. *Nucl. Eng. Des.* **14**, 390–412 (1971).
18. C. P. Berlinguette *et al.*, Revisiting the cold case of cold fusion. *Nature* **570**, 45–51 (2019).
19. N. W. Ashcroft, Metallic hydrogen: A high-temperature superconductor? *Phys. Rev. Lett.* **21**, 1748 (1968).
20. V. L. Ginzburg, Superfluidity and superconductivity in the universe. *J. Stat. Phys.* **1**, 3–24 (1969).
21. N. W. Ashcroft, Hydrogen dominant metallic alloys: High temperature superconductors? *Phys. Rev. Lett.* **92**, 187002 (2004).
22. Y. Li, J. Hao, H. Liu, Y. Li, Y. Ma, The metallization and superconductivity of dense hydrogen sulfide. *J. Chem. Phys.* **140**, 174712 (2014).
23. D. Duan *et al.*, Pressure-induced metallization of dense $(H_2S)_2H_2$ with high-$T_c$superconductivity. *Sci. Rep.* **4**, 1–6 (2014).
24. A. P. Drozdov, M. I. Eremets, I. A. Troyan, V. Ksenofontov, S. I. Shylin, Conventional superconductivity at 203 kelvin at high pressures in the sulfur hydride system. *Nature* **525**, 73–76 (2015).
25. H. Liu, I. I. Naumov, R. Hoffmann, N. W. Ashcroft, R. J. Hemley, Potential high-T_c superconducting lanthanum and yttrium hydrides at high pressure. *Proc. Natl. Acad. Sci. U.S.A.* **114**, 6990–6995 (2017).
26. F. Peng *et al.*, Hydrogen clathrate structures in rare earth hydrides at high pressures: Possible route to room-temperature superconductivity. *Phys. Rev. Lett.* **119**, 107001 (2017).
27. Z. M. Geballe *et al.*, Synthesis and stability of lanthanum superhydrides. *Angew. Chem. Int. Ed. Engl.* **57**, 688–692 (2018).
28. M. Somayazulu *et al.*, Evidence for superconductivity above 260 K in lanthanum superhydride at megabar pressures. *Phys. Rev. Lett.* **122**, 027001 (2019).
29. A. P. Drozdov *et al.*, Superconductivity at 250 K in lanthanum hydride under high pressures. *Nature* **569**, 528–531 (2019).
30. P. Kong *et al.*, Superconductivity up to 243 K in the yttrium-hydrogen system under high pressure. *Nat. Commun.* **12**, 1–9 (2021).
31. I. A. Troyan *et al.*, Anomalous high-temperature superconductivity in YH_6. *Adv. Mater.* **33**, e2006832 (2021).
32. E. Snider *et al.*, Synthesis of yttrium superhydride superconductor with a transition temperature up to 262 K by catalytic hydrogenation at high pressures. *Phys. Rev. Lett.* **126**, 117003 (2021).
33. D. V. Semenok *et al.*, Superconductivity at 253 K in lanthanum–yttrium ternary hydrides. *Mater. Today* **48**, 18–28 (2021).
34. E. Snider *et al.*, Room-temperature superconductivity in a carbonaceous sulfur hydride. *Nature* **586**, 373–377 (2020).
35. Y. Sun, J. Lv, Y. Xie, H. Liu, Y. Ma, Route to a superconducting phase above room temperature in electron-doped hydride compounds under high pressure. *Phys. Rev. Lett.* **123**, 097001 (2019).
36. R. J. Hemley, M. Ahart, H. Liu, M. Somayazulu, "Road to room-temperature superconductivity: Tc above 260 K in lanthanum superhydride under pressure" in *Proceedings of the International Symposium - Superconductivity and Pressure: A Fruitful Relationship on the Road to Room Temperature Superconductivity*, M. A. Alario-Franco, Ed. (Fundación Ramón Areces, Madrid, Spain, 2018), pp. 199–213.
37. E. Zurek, T. Bi, High-temperature superconductivity in alkaline and rare earth polyhydrides at high pressure: A theoretical perspective. *J. Chem. Phys.* **150**, 050901 (2019).
38. J. Lv, Y. Sun, H. Liu, Y. Ma, Theory-orientated discovery of high-temperature superconductors in superhydrides stabilized under high pressure. *Matter Radiat. Extrem.* **5**, 068101 (2020).
39. J. D. Benck, A. Jackson, D. Young, D. Rettenwander, Y.-M. Chiang, Producing high concentrations of hydrogen in palladium via electrochemical insertion from aqueous and solid electrolytes. *Chem. Mater.* **31**, 4234–4245 (2019).
40. S. M. Haile, C. R. Chisholm, K. Sasaki, D. A. Boysen, T. Uda, Solid acid proton conductors: From laboratory curiosities to fuel cell electrolytes. *Faraday Discuss.* **134**, 17–39, discussion 103–118, 415–419 (2007).
41. J. K. Nørskov *et al.*, Trends in the exchange current for hydrogen evolution. *J. Electrochem. Soc.* **152**, J23–J26 (2005).
42. L. Suo *et al.*, "Water-in-salt" electrolyte enables high-voltage aqueous lithium-ion chemistries. *Science* **350**, 938–943 (2015).
43. M. C. Verbraeken, C. Cheung, E. Suard, J. T. S. Irvine, High H^- ionic conductivity in barium hydride. *Nat. Mater.* **14**, 95–100 (2015).
44. H. Liu *et al.*, Dynamics and superconductivity in compressed lanthanum superhydride. *Phys. Rev. B* **98**, 100102 (2018).
45. H. Wang, Y. Yao, F. Peng, H. Liu, R. J. Hemley, Quantum and classical proton diffusion in superconducting clathrate hydrides. *Phys. Rev. Lett.* **126**, 117002 (2021).
46. L. Baggetto *et al.*, Intrinsic thermodynamic and kinetic properties of Sb electrodes for Li-ion and Na-ion batteries: Experiment and theory. *J. Mater. Chem. A Mater.* **1**, 7985–7994 (2013).
47. J. Balachandran, L. Lin, J. S. Anchell, C. A. Bridges, P. Ganesh, Defect genome of cubic perovskites for fuel cell applications. *J. Phys. Chem. C* **121**, 26637–26647 (2017).
48. J. Ding *et al.*, The influence of local distortions on proton mobility in acceptor doped perovskites. *Chem. Mater.* **30**, 4919–4925 (2018).
49. Y. Fukai, N. Okuma, Formation of superabundant vacancies in Pd hydride under high hydrogen pressures. *Phys. Rev. Lett.* **73**, 1640–1643 (1994).
50. K. Brownsberger *et al.*, X-ray diffraction, lattice structure, and equation of state of PdH_x and PdD_x to megabar pressures. *J. Phys. Chem. C* **121**, 27327–27331 (2017).
51. B. Guigue, G. Geneste, B. Leridon, P. Loubeyre, An x-ray study of palladium hydrides up to 100 GPa: Synthesis and isotopic effects. *J. Appl. Phys.* **127**, 075901 (2020).
52. J. Wellendorff *et al.*, Density functionals for surface science: Exchange-correlation model development with Bayesian error estimation. *Phys. Rev. B* **85**, 235149 (2012).
53. M. T. Cruanes, H. G. Drickamer, L. R. Faulkner, Electrochemical measurements at high pressure: Solvation and the thermodynamics of electron-transfer reactions. *J. Phys. Chem.* **96**, 9888–9892 (1992).
54. D. Giovanelli, N. S. Lawrence, R. G. Compton, Electrochemistry at high pressures: A review. *Electroanal.* **16**, 789–810 (2004).
55. Y. Ge, F. Zhang, R. P. Dias, R. J. Hemley, Y. Yao, Hole-doped room-temperature superconductivity in $H_3S_{1-x}Z_x$ (Z= C, Si). *Mater. Today Phys.* **15**, 100330 (2020).
56. I. Errea *et al.*, Quantum crystal structure in the 250-kelvin superconducting lanthanum hydride. *Nature* **578**, 66–69 (2020).
57. Z. M. Geballe *et al.*, High-pressure synthesis and thermodynamic stability of $PdH_{1\pm\varepsilon}$ up to 8 GPa. *Phys. Rev. B* **103**, 024515 (2021).
58. I. A. Kruglov *et al.*, Uranium polyhydrides at moderate pressures: Prediction, synthesis, and expected superconductivity. *Sci. Adv.* **4**, eaat9776 (2018).
59. L. Baggetto *et al.*, Characterization of sodium ion electrochemical reaction with tin anodes: Experiment and theory. *J. Power Sources* **234**, 48–59 (2013).
60. J. A. Flores-Livas *et al.*, A perspective on conventional high-temperature superconductors at high pressure: Methods and materials. *Phys. Rep.* **856**, 1–78 (2020).
61. J. J. Mortensen, L. B. Hansen, K. W. Jacobsen, Real-space grid implementation of the projector augmented wave method. *Phys. Rev. B* **71**, 035109 (2005).
62. J. Enkovaara *et al.*, Electronic structure calculations with GPAW: A real-space implementation of the projector augmented-wave method. *J. Phys. Condens. Matter* **22**, 253202 (2010).
63. A. Hjorth Larsen *et al.*, The atomic simulation environment–A Python library for working with atoms. *J. Phys. Condens. Matter* **29**, 273002 (2017).
64. P. Vinet, J. R. Smith, J. Ferrante, J. H. Rose, Temperature effects on the universal equation of state of solids. *Phys. Rev. B* **35**, 1945–1953 (1987).
65. P. Linstrom, W. Mallard, Eds., *NIST Chemistry WebBook, NIST Standard Reference Database Number 69* (National Institute of Standards and Technology, 2018).
66. Y. Wang, J. Lv, L. Zhu, Y. Ma, Crystal structure prediction via particle-swarm optimization. *Phys. Rev. B* **82**, 094116 (2010).
67. Y. Wang, J. Lv, L. Zhu, Y. Ma, CALYPSO: A method for crystal structure prediction. *Comput. Phys. Commun.* **183**, 2063–2070 (2012).
68. J. P. Perdew, K. Burke, M. Ernzerhof, Generalized gradient approximation made simple. *Phys. Rev. Lett.* **77**, 3865–3868 (1996).
69. K. Lee, É. D. Murray, L. Kong, B. I. Lundqvist, D. C. Langreth, Higher-accuracy van der Waals density functional. *Phys. Rev. B* **82**, 081101 (2010).
70. S. P. Ong *et al.*, Python Materials Genomics (pymatgen): A robust, open-source python library for materials analysis. *Comput. Mater. Sci.* **68**, 314–319 (2013).
71. T. F. Willems, C. H. Rycroft, M. Kazi, J. C. Meza, M. Haranczyk, Algorithms and tools for high-throughput geometry-based analysis of crystalline porous materials. *Microporous Mesoporous Mater.* **149**, 134–141 (2012).
72. P.-W. Guan, R. J. Hemley, V. Viswanathan, Pressure-potential phase diagrams of metal-hydrogen. GitHub. https://github.com/BattModels/P2. Deposited 28 October 2021.